

See discussions, stats, and author profiles for this publication at: <https://www.researchgate.net/publication/258931939>

# Influence of Charged Polypeptides on Nucleation and Growth of CaCO<sub>3</sub> Evaluated by Counterdiffusion Experiments

ARTICLE in CRYSTAL GROWTH & DESIGN · JULY 2013

Impact Factor: 4.89 · DOI: 10.1021/cg400523w

---

CITATIONS

10

READS

19

## 7 AUTHORS, INCLUDING:



[María Sancho-Tomás](#)

SOLEIL synchrotron - Institut de Physique du ...

6 PUBLICATIONS 34 CITATIONS

[SEE PROFILE](#)



[Simona Fermani](#)

University of Bologna

79 PUBLICATIONS 1,316 CITATIONS

[SEE PROFILE](#)



[Miguel A. Durán-Olivencia](#)

Imperial College London

13 PUBLICATIONS 48 CITATIONS

[SEE PROFILE](#)



[Juan M. Garcia-Ruiz](#)

University of Granada

285 PUBLICATIONS 4,454 CITATIONS

[SEE PROFILE](#)

# Influence of Charged Polypeptides on Nucleation and Growth of $\text{CaCO}_3$ Evaluated by Counterdiffusion Experiments

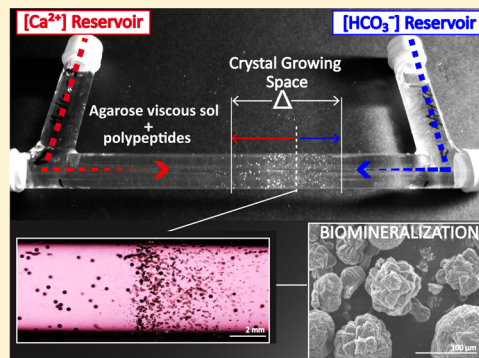
M. Sancho-Tomás,<sup>†</sup> S. Fermani,<sup>‡</sup> Miguel A. Durán-Olivencia,<sup>†</sup> F. Otálora,<sup>†</sup> J. Gómez-Morales,<sup>\*,†</sup> G. Falini,<sup>\*,‡</sup> and J. M. García-Ruiz<sup>†</sup>

<sup>†</sup>Laboratorio de Estudios Cristalográficos, IACT (CSIC-UGR), Avda. Las Palmeras, no. 4. E-18100 Armilla, Spain

<sup>‡</sup>Dipartimento di Chimica "G. Ciamician", Alma Mater Studiorum Università di Bologna, via Selmi 2, I-40126 Bologna, Italy

## Supporting Information

**ABSTRACT:** Many mineralization processes occur in convection-free conditions. Understanding these processes requires knowledge of crystal nucleation and growth processes in gels or high viscous sol systems. In this work, the crystallization parameters of calcium carbonate in an agarose viscous sol using counterdiffusion crystallization were monitored as a function of time. Additionally, by comparing the precipitation parameters in the high viscous sol entrapping charged polypeptides, namely, poly-L-lysine (pLys), poly-L-aspartate (pAsp), and poly-L-glutamate (pGlu), it was possible to establish the polypeptide capability to inhibit, or eventually promote, the calcium carbonate nucleation and/or crystal growth processes. The polymorphism and morphology of the precipitates indicate that pLys only influences the growth mechanism of calcium carbonate without affecting the nucleation process. On the contrary, pAsp and, to a minor extent, pGlu affect both nucleation and growth. The application of this analysis can be extended to other additives and macromolecules able to affect crystallization processes.



## 1. INTRODUCTION

Precipitation processes are strongly affected by the presence of additives, which can not only promote, slow down, or inhibit nucleation and growth but also affect the selective formation of a polymorph or produce a morphological change.<sup>1–3</sup> An evaluation of their effects on nucleation and growth processes is of key importance for a wide range of applications, particularly, in the case of calcium carbonate ( $\text{CaCO}_3$ ), for their use as antiscalining agents<sup>4</sup> or as molecular models for understanding biominerization processes.<sup>5</sup> The additives' action can be exerted in the stage of nucleation or growth, or in both stages. The influence on these crystallization stages is usually studied analyzing kinetics curve profiles, reporting the variation of supersaturation, or a related parameter, with time.<sup>6</sup> Usually, in doing this approach, the precipitating system is started at a high initial supersaturation value, which then decreases as the precipitation occurs. This approach offers several advantages, one of the most important being the possibility to follow the formation of intermediates or transition phases. However, to study the role of different starting supersaturations, it is necessary to set up different batch experiments. An alternative is the use of the gel technique, in particular, with the counterdiffusion configuration (CDS), often called the double diffusion system. In a typical counterdiffusion experiment, two reacting solutions are allowed to diffuse against each other from two reservoirs separated by a gel column. This configuration generates a continuous gradient of concentrations of both reagents in the gel column and, therefore, a continuous variation in space and time of the ionic activity product of the

reactants and supersaturation.<sup>7,8</sup> The flow rate of reactants across the gel not only is a function of their diffusion coefficient in water but also depends on the ionic strength of the solution and on the gel strength or viscosity.

The concentration gradient of the reactants in space and time can be obtained from Fick's second law using estimated values of the diffusion coefficients. Supersaturation values can then be easily estimated from the ratio of the ionic activity product (IAP) of the reactants and the solubility product ( $K_{\text{sp}}$ ) of the compound formed by the reaction. Therefore, precipitation will occur at the time and location of the gel column where the critical supersaturation value for nucleation is reached for the first time.<sup>9–16</sup> However, it should be noticed that (a) the value of the supersaturation threshold to trigger nucleation is a function of the rate of development of supersaturation<sup>10–14</sup> and (b) the equivalence rule must be satisfied in addition to reaching the supersaturation threshold.<sup>10,11,13–16</sup>

CDS also allows studying the crystallization in the pore space of the gel network. The pore volume can be varied by controlling the entanglement parameters, such as pH in silica gels<sup>17</sup> or the concentration of ions<sup>18</sup> and macromolecules<sup>19</sup> in polysaccharide gels. Agarose forms gels with different strengths depending on its concentration.<sup>19</sup> This gel has a structure almost independent from the pH and the presence of foreign ions.

Received: April 9, 2013

Revised: July 22, 2013

Published: July 26, 2013



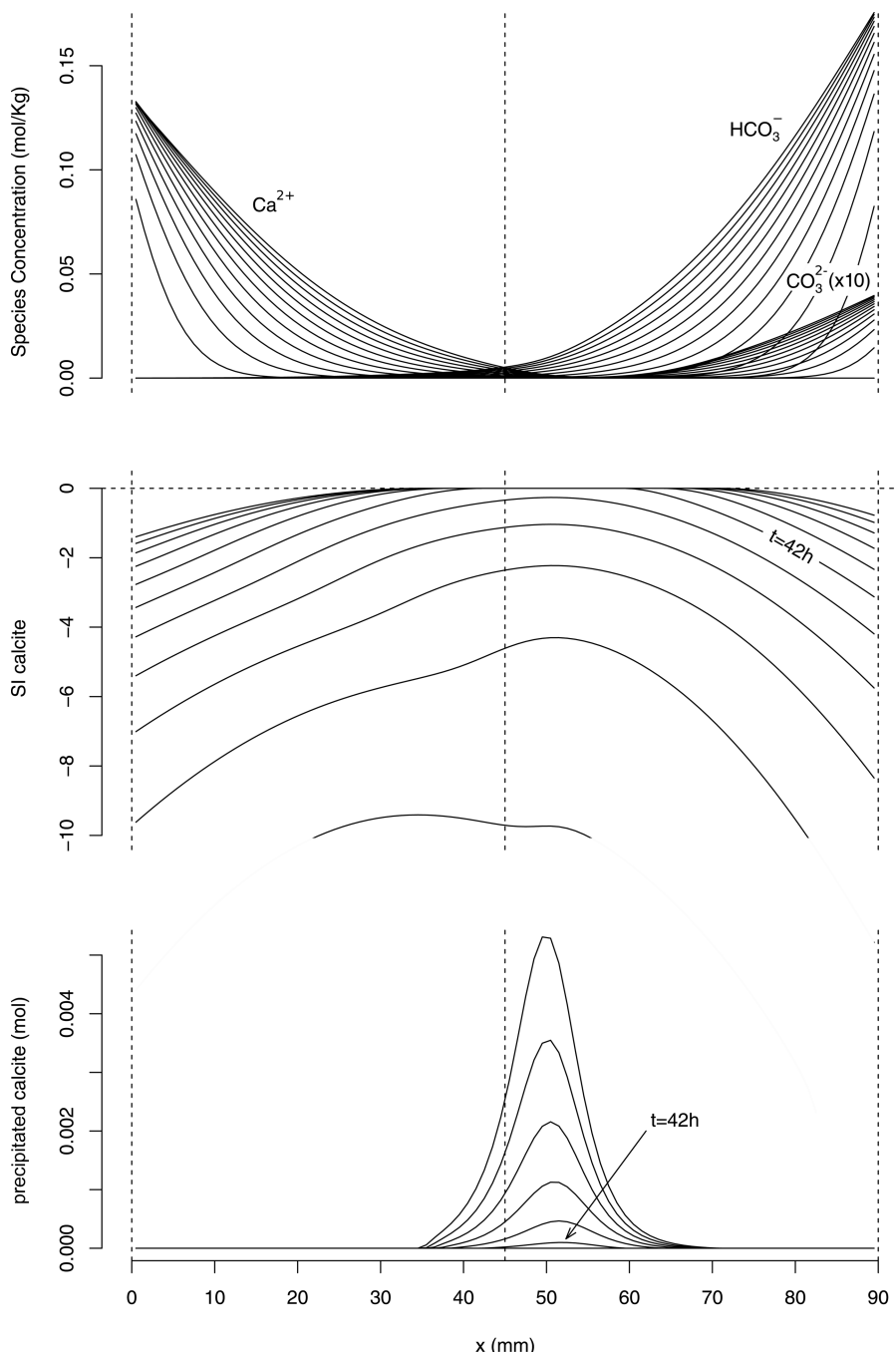


**Figure 1.** Output of the PHREEQC simulation:  $\text{Ca}^{2+}$ ,  $\text{HCO}_3^-$ , and  $\text{CO}_3^{2-}$  concentrations (top), saturation index with respect to calcite (middle), and amount of precipitated calcite (bottom) within the tube as a function of the position ( $x$ ) at different times (from 12 to 72 h; lines represent each 6 h). The vertical dashed lines indicate the beginning, middle, and end of the tube. The first line in the saturation index (S.I.) evolution plot corresponds to 12 h. The first visible maximum in the precipitated calcite plot corresponds to 42 h. This maximum, normalized by the length of the tube, is located around  $x = 0.58$ .

The use of gels as crystallization media and, in particular, in the CDS technique, which allows one to screen in a single experiment a wide range of crystallization conditions, have been the reasons that trigger the interest in many different fields ranging from optimization of crystal size and crystal quality,<sup>7,8,20–24</sup> simulation of microgravity environments,<sup>20</sup> analogous of geological environments,<sup>25,26</sup> production of biomimetic materials,<sup>27,28</sup> and to mimic biominerization.<sup>29–34</sup>

All of these studies allow controlled crystallization of a plethora of minerals, among them calcium phosphates<sup>32,34,35</sup> and

calcium carbonates,<sup>27,29,30,36,37</sup> along with the study of the effects of inorganic and organic additives on these crystallization processes.<sup>36,37</sup> The aforementioned investigations have mainly focused on the analysis of the size, habit, and quality of the grown crystals, but few of them have focused on monitoring the precipitation process as a function of time. In this paper, we report the monitoring in time and space of the crystallization of calcium carbonate in agarose viscous sols.<sup>38</sup> By entrapping different organic additives in agarose viscous sols, we have measured the variation of the relevant parameters defining the

precipitation kinetics of the CDS. This allowed us to evaluate the inhibiting capability of organic additives (namely, charged polypeptides, pLys, pAsp, and pGlu) over the nucleation, growth, habit, and polymorphic phases of calcium carbonate crystals.

## 2. THEORETICAL CONSIDERATIONS ON A PRECIPITATION EXPERIMENT IN GEL USING THE COUNTERDIFFUSION SYSTEM

**2.1. Numerical Simulation of Ion Concentration Gradients, Supersaturation, and Location of the Initial Precipitate.** During a CDS experiment, the precipitation of a given phase occurs in a convection-free gel environment, and therefore, the transport processes are solely controlled by diffusion. The reservoirs of the reagents' solutions act as semi-infinite sources of ions, creating time-dependent gradients of concentrations along the gel. When the initial concentration of diffusing reagents in the reservoirs is the same, we would expect an increase of the ion activity product at the center of the gel column, eventually leading to the threshold value for nucleation (i.e., critical supersaturation).<sup>7–12</sup>

The numerical simulation of time-dependent ion concentration gradients and saturation indexes as well as the location of the initial  $\text{CaCO}_3$  precipitate in the additive-free experiment has been done with PHREEQC (see the Materials and Methods section for further details). The results of such simulations are plotted in Figure 1, with a common  $x$  axis corresponding to the tube length. The concentration gradients of  $\text{Ca}^{2+}$ ,  $\text{HCO}_3^-$ , and  $\text{CO}_3^{2-}$  are plotted in the top panel, whereas the evolution of the saturation index (S.I.) in space and time is represented in the middle one. For clarity, the concentration gradients of the rest of the species, including ions and pairs, are not represented. As soon as the IAP in this system overcomes the  $K_{\text{sp}}$  of calcite, at a particular region of the gel column, a precipitate in that zone appears and S.I. is reduced to 0. We can observe at the bottom panel, representing the amount of precipitated calcite, the first visible maximum produced after 42 h of experiment and located at 53 mm from the  $\text{Ca}^{2+}$  reservoir (normalized length = 0.58). At increased periods of time, as the ionic diffusion continues, the precipitated mass of calcite increases, progressively reducing S.I. to 0. The shift of the maximum toward the anion reservoir indicates the unbalanced concentration of the two reactants solutions, the anionic being the limiting one.

**2.2. Definition and Interpretation of the Measured Parameters.** A CDS allow us to assess the main parameters involved in a mineral precipitation process (Figure 2). The starting point of crystallization,  $x_o$ , is defined as the distance from the cationic reservoir to the first observed precipitate. This is the point where the equivalence rule has to be fulfilled and the ion activity product exceeds the critical value needed to yield nucleation and further growth.<sup>10,11,13–16</sup> The waiting time,  $t_w$ , refers to the time that elapses from the onset of the experiment to the observation of the first crystals with an optical polarized microscope using a 4 $\times$  objective. At constant volume,  $t_w$  can be considered inversely proportional to the nucleation frequency and, therefore, represents an indirect estimation of the supersaturation, and consequently of the critical activities needed to sustain nucleation and growth. The crystal growing space ( $\Delta$ ) is the length of the region in the gel tube in which crystals are observed at the end of the experiment.  $\Delta$  can be not symmetric around  $x_o$ ; in this case, the growing space from  $x_o$  to the last observed crystals in the direction of the cationic reservoir ( $\Delta_{\text{cat}}$ ) is

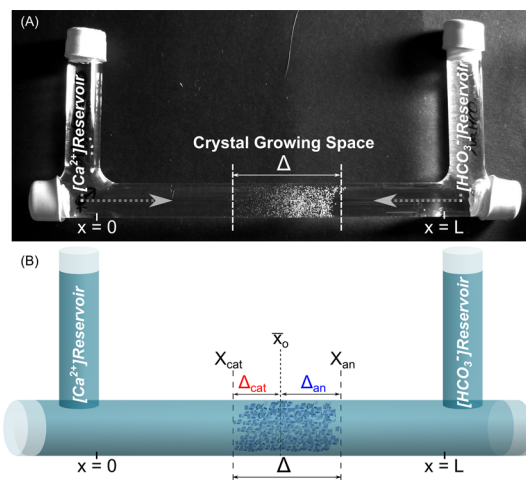


**Figure 2.** (a) Photograph of the U-tube setup used for  $\text{CaCO}_3$  crystallization experiments in CDS using agarose viscous sols. (b) Schematic illustration of the measured crystallization parameters in the U-tube:  $x_o$ , the starting crystallization point;  $\Delta$ , the crystal growing space;  $x_{\text{cat}}$  and  $x_{\text{an}}$ , the boundaries of the crystal growing space close to the cationic and anionic reservoirs, respectively;  $\Delta_{\text{cat}}$  and  $\Delta_{\text{an}}$ , the crystal growing space from the starting point to the cationic and anionic reservoirs, respectively.

different from that to the anionic one ( $\Delta_{\text{an}}$ ). The boundaries of  $\Delta$ ,  $x_{\text{cat}}$  and  $x_{\text{an}}$  represent, respectively, the places where the activity of anions in the zone close to the cationic reservoir and the activity of cations in the zone close to the anionic one are the lowest to still sustain nucleation and growth of crystals. The asymmetry of  $\Delta$  with respect to  $x_o$  suggests a different range of ionic activity of cations and anions to sustain nucleation and growth. The crystallization density,  $d_o$ , represents the number of observed crystals by optical microscope per unit of volume. As long as the counting of crystals in the CDS is not a trivial issue, a qualitative scale was defined (Figure S1, Supporting Information): low density indicates that crystals are well separated one from another; medium density corresponds to a view in which crystals can still be observed as single units, but they partially overlap; high density represents a massive precipitation in which single crystals are not distinguishable anymore. This parameter ( $d_o$ ) is important since it is an indirect measure of the frequency of nucleation, assuming that a strong inhibition of growth is not present. The crystal size was also considered, although, in many cases, we found it impossible to measure due to an overlap of the particles.

All of these parameters are a function of the boundary conditions, that is, concentration of the reservoir solutions, nature and degree of entanglement of the gel, length and cross section of the gel tube, temperature, and final time of the experiment. They are supposed to be constant in comparative experiments in which additives are present in the gel or in one of the reservoir solutions.

**2.3. Role of Additives Entrapped in the Gel During a CDS Precipitation Process.** For clarity, we suppose that the presence of entrapped additives does not alter the diffusion coefficients of the precipitating ions. This assumption can be considered valid when a small amount of additives is entrapped in the viscous sol. The comparison among measurable parameters in the absence and presence of entrapped additive allows assessment of their promoting or inhibiting effect on the nucleation and/or growth of crystals.

An inhibition or slowdown of the nucleation process produced by adsorption of the additives on the first formed

nuclei (or even on prenucleation clusters) of a given mineral phase can cause a rise of  $t_w$  along with a reduction of  $\Delta$ , while  $x_o$  should remain fixed. As the ion diffusion continues, this process leads to an increase of the actual ion activity product (i.e., supersaturation) in the bulk of the gel. An increase of the density of nucleation ( $d_c$ ) is also expected since the nucleation rate is a (negative) exponential function of supersaturation. The presence of  $\Delta$  asymmetry can be justified, for  $\text{CaCO}_3$ , as follows. After the starting of the precipitation process, the pH in the precipitation region decreases, due to the decrease of the ionic activity product to the solubility product. This provokes a change in the speciation of the carbonate/hydrogen carbonate ions in favor of the latter. Thus, a shorter growing space in the direction of the calcium reservoir with respect to the hydrogen carbonate one is observed. This effect is enhanced by the presence of the polypeptides, which increase the saturation index threshold necessary for nucleation, measured as waiting time.

An inhibition of the growth process should not affect the  $d_c$  and  $\Delta$  values, but the size, growth morphology, and aggregation of the crystals. The presence of inhibition on nucleation and growth should cause an increase of  $t_w$  and a decrease of  $\Delta$  with higher  $d_c$ , and leave  $x_o$  unchanged. Moreover, the crystal morphology should change. The increase of supersaturation at which nucleation and growth can occur in a precipitation process inhibited by soluble additives may also provoke the precipitation of a second phase, usually a polymorph with higher solubility. In this case, the comparison cannot be done with a system in which the precipitation of a less soluble phase takes place.

### 3. MATERIALS AND METHODS

**3.1. Numerical Simulations of the CDS Experiment.** A simplified simulation has been designed to capture the complex behavior of simultaneous multicomponent mass transport, chemical speciation, and nucleation/growth kinetics. Since the subtleties of such a simulation can grow up to the point of obscuring the discussion of the experimental results presented, some simplifications have been made, particularly in the nucleation kinetics in the metastable zone, because the resulting loss of accuracy is largely outweighed by the clarity in the discussion and the ease of appraisal of our results by nonspecialists in counterdiffusion.

Ionic transport, evolution of supersaturation (as saturation index, S.I. =  $\log(\text{IAP}/K_{sp})$ ), and the region of initial precipitation of  $\text{CaCO}_3$  in the absence of additives were simulated using closed boundary, multicomponent diffusion of each solute constrained by the overall charge balance.<sup>39,40</sup> The simulation was implemented in PHREEQC 2.18.3<sup>41</sup> using 150 cells (1 mm each) and 1 s time steps. Advective transport was disabled. Speciation and equilibrium calcite precipitation/dissolution (at S.I. = 0) was also computed by PHREEQC using the default values in the phreeqc.dat database.

**3.2. Preparation of Agarose Viscous Solns.** First, an agarose solution stock of 0.2% (w/v) was heated to 90 °C for 20 min to dissolve completely the agarose powder (Agarose D-S, Hispanagar). The solution was then cooled to 65 °C and thereafter mixed with the required volume of heated milli-Q water (resistivity = 18.2 MΩ·cm at 25 °C; filtered through a 0.22 μm membrane) to obtain a final 0.1% (w/v) agarose solution. An equal volume of this solution was poured in four different beakers. In each beaker, an amount of poly-L-aspartic acid sodium salt (MW 9600 Da; Sigma-Aldrich), poly-L-glutamic acid sodium salt (MW 9600 Da; Sigma-Aldrich), or poly-L-lysine hydrochloride (15 000 Da; Sigma-Aldrich) was added to reach a final concentration of 20 μg/mL. The prepared solution was shaken during 1–2 min and then added to the different U-tubes with a 5 mL syringe. The starting pH of the agarose viscous non-Newtonian sol<sup>38</sup> was always 6.5, regardless of the presence or absence of entrapped polypeptides.

**3.3. Calcium Carbonate Crystallization System.** The experiments were carried out by using a U-tube system (Triana Science & Technology, S.L., Figure 2). The U-tube has a column length of 90 mm that is accessible to diffusing reagents from two side source reservoirs. In the cation reservoir, 1 mL of a 0.5 mol·L<sup>-1</sup>  $\text{CaCl}_2$  (pH = 5.7) solution prepared from  $\text{CaCl}_2 \cdot 2\text{H}_2\text{O}$  (Sigma-Aldrich) was added, whereas 1 mL of 0.5 mol·L<sup>-1</sup>  $\text{NaHCO}_3$  (pH = 8.15 ± 0.10) prepared from  $\text{NaHCO}_3$  (Fluka Biochemika) was added in the anion reservoir.  $\text{CaCl}_2$  and  $\text{NaHCO}_3$  solutions diffused one against the other through the column filled with an agarose viscous sol entrapping the polypeptides. When the first crystals appeared in each U-tube, we measured the distance from the cationic reservoir to  $x_o$  and the length of  $\Delta$  14 days after. Precipitates were recovered from the column tube and filtered by using a 0.45 μm pore size membrane. Once in the filter, they were washed several times with hot milli-Q water in order to remove the agarose residue and then dried at room temperature. All the experiments were performed at room temperature (22 ± 3 °C) and were repeated at least three times.

**3.4. Characterization of  $\text{CaCO}_3$  Precipitates.** Fourier transform infrared (FTIR) spectra of samples in KBr disks were collected at room temperature by using a FTIR Nicolet 380 Thermo Electron Corporation spectrophotometer working in the range of wavenumbers 4000–400 cm<sup>-1</sup> at a resolution of 2 cm<sup>-1</sup>. A finely ground, approximately 1% (w/w) mixture of the sample in KBr, was pressed into a transparent disk using a hydraulic press and applying a pressure of 48.6 psi. X-ray powder diffraction patterns were collected using a Panalytical X'Pert MPD diffractometer provided of  $\text{Cu K}\alpha$  radiation. The diffraction patterns were collected within the 2θ range from 10° to 60°. The optical microscope (OM) observations were made with a Leika optical microscope equipped with a digital camera. As-prepared samples were inspected in a Phenom scanning electron microscope (SEM). In addition, scanning electron micrographs of gold-sputtered samples were recorded using a Hitachi FEG 6400 scanning electronic microscope.

### 4. RESULTS

In Figure 3, pictures of crystal growing spaces ( $\Delta$ ) of the different crystallization U-tubes are shown. The parameters measured during the crystallization experiment are also graphically reported and summarized in Table 1.

A reference experiment was carried out in the absence of polypeptides entrapped in the agarose viscous sol. The cationic reservoir contained a 0.5 mol·L<sup>-1</sup> calcium chloride solution and the anionic one a 0.5 mol·L<sup>-1</sup> hydrogen carbonate solution. In this experiment,  $t_w$  was around 2 days (1.8 ± 0.5) at an  $x_o$  position equal to 0.66 ± 0.12. The precipitation evolved asymmetrically with respect to  $x_o$ , and after 15 days,  $\Delta_{\text{cat}}$  and  $\Delta_{\text{an}}$  were equal to 0.10 and 0.16, respectively, resulting in a  $\Delta$  of 0.26 (Table 1). The precipitate showed a low  $d_c$  in the  $\Delta_{\text{cat}}$  region and a medium one in the  $\Delta_{\text{an}}$  region. Under this particular condition, calcite was the only phase precipitated, as detected by FTIR spectroscopy and X-ray powder diffraction profiles (Figure 4) in which the only typical absorption bands at 1422 ( $\nu_3$ ), 875 ( $\nu_4$ ), and 712 cm<sup>-1</sup> ( $\nu_2$ ) and diffraction peaks at 23.0° (012), 29.4° (104), 35.9° (110), 47.5° (018), and 48.5° (116) were observed, respectively.<sup>42,43</sup> Calcite appeared as single crystals of sizes between 200 and 300 μm displaying rhombohedral {10.4} faces plus less extended {hk.0} faces (Figure 5 and Figure S12, Supporting Information).

When pLys was entrapped in the gel,  $x_o$  was 0.68 ± 0.09 and  $\Delta$  was 0.29.  $\Delta_{\text{cat}}$  (0.11) was shorter than  $\Delta_{\text{an}}$  (0.18), and the  $t_w$  was around 4 days (3.7 ± 0.5). The  $d_c$  was high in the central region of  $\Delta$ , low in the  $\Delta_{\text{cat}}$  region, and medium in the  $\Delta_{\text{an}}$  one. In this case, the FTIR spectrum and the X-ray powder diffraction pattern showed additional bands at 1467, 855, and 700 cm<sup>-1</sup> and diffraction peaks at 26.2° (111), 27.2° (021), 38.6° (022), and 45.9° (211), with respect to those from the

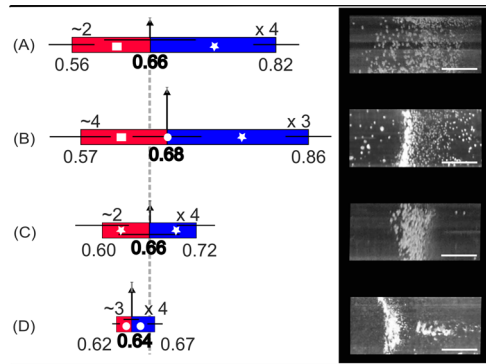


**Figure 3.** Left: Graphical representation of the measured parameters in the precipitation experiments of calcium carbonate by CDS. The length of the tube has been normalized from cation reservoir (0) to anion reservoir (1). The real length of the tube was 90 mm. Red and blue colors indicate the crystallization region from the starting point of crystallization ( $x_o$ , bold numbers) to the cation reservoir ( $x_{cat}$ , left-lower corner) and anion reservoir ( $x_{an}$ , right-lower corner), respectively. Arrows indicate the waiting time ( $t_w$ , left-upper corner), and the number of replicas is shown in the right-upper corner. Horizontal black lines in the middle of each figure and vertical gray lines on the arrow show the variability in the measures. Crystallization density (see Figure SI1, Supporting Information) is represented as squares (low), stars (medium), and circles (high). Right: Photographs of the crystal growing spaces ( $\Delta$ ) after 15 days crystallization time under conditions of counterdiffusion in the presence of charged polypeptides entrapped in agarose viscous sols. Scale bar: 5 mm.

reference experiment (Figure 4), thus indicating the presence of aragonite<sup>42,43</sup> plus calcite. Calcite appeared as aggregates of modified rhombohedra crystals having sizes in the range of 200–500  $\mu\text{m}$ . The constituting crystalline units of the aggregates showed rough surfaces almost not showing the typical {10.4} faces. Aragonite crystallized well embedded in the agarose viscous sol as spherulites terminated by needles. The size of aragonite spherulites, 50–100  $\mu\text{m}$ , suggests that they were formed in the  $\Delta_{an}$  region (Figure 3, right). In the presence of entrapped pGlu in the agarose viscous sol, the  $x_o$  value was of  $0.66 \pm 0.08$  and the  $t_w$  was about 2 days ( $1.8 \pm 0.9$ ).  $\Delta$  was 0.12 and almost symmetric around  $x_o$ . The FTIR spectrum and the X-ray powder diffraction pattern showed only bands and peaks characteristic of calcite (Figure 4). The  $d_c$  was medium in all the  $\Delta$  region. Highly faceted rhombohedral crystals of calcite of about

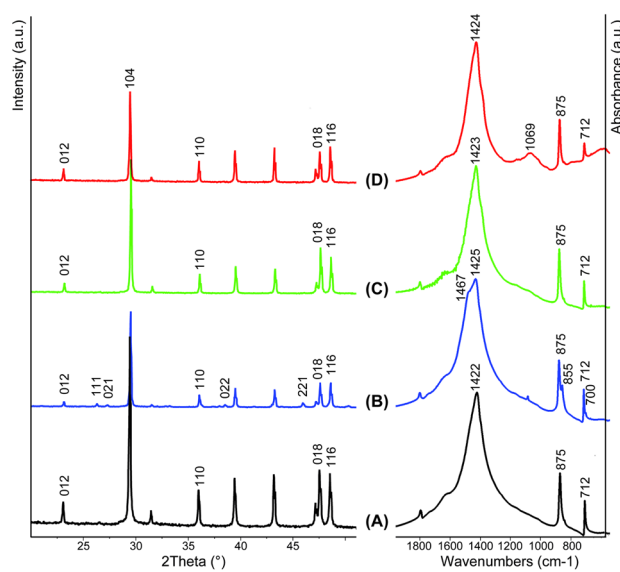


**Figure 4.** X-ray powder diffraction patterns (left) and FTIR spectra (right) of  $\text{CaCO}_3$  precipitated into the agarose viscous sol entrapping pLys (B), pGlu (C), or pAsp (D), and in the absence of additive (A). The absorption of the FTIR bands is reported in arbitrary units (a.u.). The diffraction patterns are displaced along the  $y$  axis that reports intensity in arbitrary units (a.u.).

180–250  $\mu\text{m}$  precipitated, displaying rhombohedral {10.4} faces together with extended {hk.0} faces.

When pAsp was entrapped in the agarose viscous sol,  $x_o$  was of  $0.64 \pm 0.02$  and  $t_w$  was about 3 days ( $2.8 \pm 0.9$ ).  $\Delta_{cat}$  was similar to  $\Delta_{an}$ , 0.02 and 0.03, respectively, resulting in a  $\Delta$  of 0.05. The density of crystallization,  $d_c$ , in this short region is high. The FTIR spectra and the X-ray powder diffraction pattern show only the presence of calcite. These calcite particles precipitated as irregular aggregates formed by distorted rhombohedra with sizes between 100 and 250  $\mu\text{m}$  grouped in a radial way. The morphology of these single crystals is prismatic having elongated {hk.0} faces and capped by rhombohedral {10.4} faces.

## 5. DISCUSSION

The counterdiffusion technique can be used to monitor the effects of increasing the ionic concentration during the

**Table 1. Summary of Data from Precipitation Experiments of Calcium Carbonate by CDS in the Absence of Additives and in the Presence of pLys, pGlu, or pAsp Entrapped in the Agarose Viscous Sol<sup>g</sup>**

|      | crystallization parameters |             |                 |         |                |     | precipitate features |                           |                   |
|------|----------------------------|-------------|-----------------|---------|----------------|-----|----------------------|---------------------------|-------------------|
|      | $\Delta_{cat}^a$           | $x_o^a$     | $\Delta_{an}^a$ | $t_w^b$ | $d_c^c$        | no. | phase <sup>d</sup>   | shape <sup>e</sup>        | size <sup>f</sup> |
| ref. | 0.10 (0.06)                | 0.66 (0.12) | 0.16 (0.06)     | ~2      | <i>l, m</i>    | 4   | C                    | <i>rhomb.</i>             | 200–300           |
| pLys | 0.11 (0.08)                | 0.68 (0.09) | 0.18 (0.06)     | ~4      | <i>l, m, h</i> | 3   | C, A                 | <i>r. aggreg.; spher.</i> | 200–500 50–100    |
| pGlu | 0.06 (0.07)                | 0.66 (0.08) | 0.06 (0.05)     | ~2      | <i>m</i>       | 4   | C                    | <i>facet rh.</i>          | 180–250           |
| pAsp | 0.02 (0.01)                | 0.64 (0.02) | 0.03 (0.02)     | ~3      | <i>h</i>       | 4   | C                    | <i>r. aggreg.; pean.</i>  | 100–250           |

<sup>a</sup>These values are normalized with respect to the length of the U-tube from the cation (0) to the anion reservoir (1). Their associated standard deviations are reported in parentheses. <sup>b</sup>The  $t_w$  is measured in days. <sup>c</sup>The  $d_c$  is defined by a qualitative scale: low (*l*), medium (*m*), and high (*h*) (see Figure SI1, Supporting Information). <sup>d</sup>Precipitated mineral phase: C and A indicate calcite and aragonite, respectively. <sup>e</sup>Morphology of crystals observed by SEM: *rhomb.* indicates modified rhombohedra; *r. aggreg.* indicates aggregates of modified rhombohedra; *spher.* indicates spherulites; *facet rh.* indicates highly facet modified rhombohedra; *pean.* indicates peanut-like shape. <sup>f</sup>The size of the particles ( $\mu\text{m}$ ) refers to the longest axis. <sup>g</sup>The crystallization parameters refer to measures of the mineral precipitation in the U-tube: starting point of crystallization ( $x_o$ ); length of the region around  $x_o$  ( $\Delta = \Delta_{cat} + \Delta_{an}$ ) versus cationic ( $\Delta_{cat}$ ) and anionic ( $\Delta_{an}$ ) reservoirs; waiting time ( $t_w$ ); crystallization density ( $d_c$ ); number of replicas for each condition (no.). The precipitate features refer to the calcium carbonate phase, shape, and size of crystals as recorded at the end of the crystallization experiment after removal from the agarose.

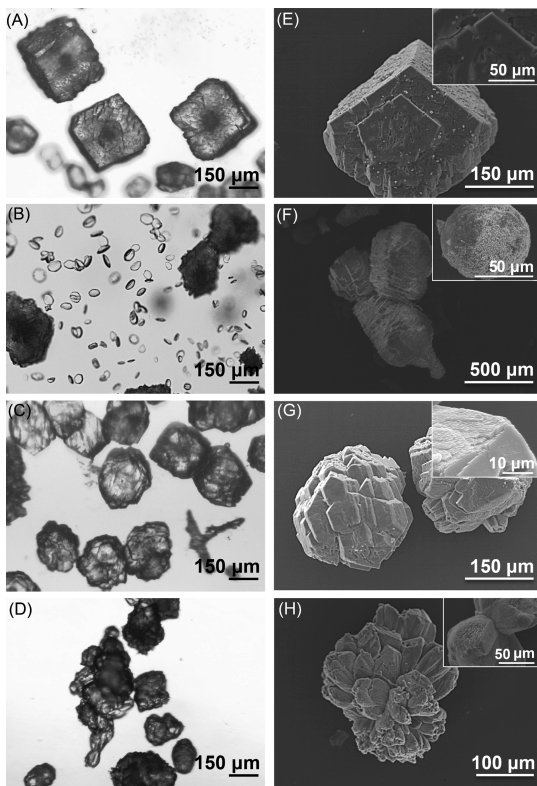


**Figure 5.** Morphology of calcium carbonate crystals formed in the agarose viscous sols in the absence of additives (A, E) and in the presence of entrapped pLys (B, F), pGlu (C, G), and pAsp (D, H). (A–D) Optical microscope pictures of the calcium carbonate crystals immersed in the agarose viscous sol and SEM pictures (E–H) of the same crystals after removal from the agarose. The inset in (F) shows a spherulite of aragonite, whereas those in (E), (G), and (H) show high magnification of the calcite crystals. These crystals are representative of the whole sample populations.

precipitation of salts over the time, under conditions controlled exclusively by diffusion. By applying the theoretical principles,<sup>7–12</sup> which govern the crystallization process in gel systems, it is possible to assess the effects of an entrapped additive on the nucleation and growth processes of a given salt through CDS experiments. The influence of additives in gel crystallization has been poorly investigated so far, while more attention has been paid to the effects of the temporal increasing ion activities on the morphological evolution of the precipitates.<sup>29–32,36,37</sup>

The potential of the CDS has been used to study the precipitation of  $\text{CaCO}_3$  in agarose viscous sols in the presence of charged polypeptides as additives due to their relevance in scaling and biominerization processes.<sup>4,5</sup> The position of  $x_o$  has to fulfill the equivalence rule.<sup>10,11,13–16</sup> Thus, it is a function of the concentration of  $\text{Ca}^{2+}$  and  $\text{CO}_3^{2-}$  ions. As the pH of the hydrogen carbonate solution was  $8.15 \pm 0.10$ , the estimated molar fraction of carbonate ions in the anionic reservoir was about 1.5% of the total carbonate. In all experiments, both in the absence or in the presence of entrapped additives, the pH of the agarose assumed the value of 6.5. The agarose viscous sol was not buffered, so its pH changed during the ionic diffusion process and, from the above data, appeared governed by the diffusion of  $\text{HCO}_3^-$  and  $\text{CO}_3^{2-}$  ions. The fact that the starting point of crystallization was around  $x_o = 0.66$  in all experiments is a consequence of the lower concentration of  $\text{CO}_3^{2-}$  with respect to that of  $\text{Ca}^{2+}$  (about 1.5%). As a consequence of the

nonstoichiometry of reagent concentration,  $x_o$  has to shift from the center of the tube toward the anionic reservoir (limiting reactant) in order to fulfill the equivalence rule. In this respect, the speciation software PHREEQC successfully predicted this shift, and the place of initial precipitation roughly coincided with  $x_o$  observed experimentally. Another interesting observation was the appearance of the first visible maximum in the amount of precipitated calcite at 30 h (Figure 1) in contrast to the experimentally observed  $t_w$  of around 2 days. This is explained by the following reasons: first,  $t_w$  considers not only the nucleation time  $t_n$  but also the growth time  $t_g$ . Second, the simulation does not include nucleation as a process where a potential barrier must be overcome and which happens at S.I. values larger than 0. Third, the speciation software does not simulate the important effect of the nonstoichiometry of the reagent composition on the time for the appearance of the first precipitate, as demonstrated in equivalent batch experiments in which  $t_w$  ( $[\text{Ca}^{2+}]/[\text{C}_T] \# 1$ ) was higher than  $t_w$  ( $[\text{Ca}^{2+}]/[\text{C}_T] = 1$ ).<sup>44</sup>

The carbonate speciation related effect also justifies the asymmetry of  $\Delta$ , as a consequence of the longer crystallization space in the direction of the anionic reservoir with respect to the cationic one, as also predicted by the theoretical study carried out. It is worth mentioning that the borders of  $\Delta$  are determined by the concentration in the reservoirs and the required conditions of supersaturation and critical ion concentration to sustain the crystallization process.

The  $x_o$  position depends on the speciation of calcium and carbonate ions. Since the addition of pAsp, pGlu, and pLys with different charge ( $pK_a$ ) to the agarose viscous sol did not significantly change the  $x_o$  position, we may infer that the speciation of calcium and carbonate ions was not affected by these additives. This is an important point to have in mind when studying the effect of entrapped additives on the precipitation of salts within a viscous solution during a CDS experiment. However,  $t_w$  increased in the cases of pAsp and pLys with respect to the reference. A longer  $t_w$  implies an increase of the ionic activity product, which leads the possibility of the precipitation of more soluble polymorphs. That is what occurs in the case of pLys, where calcite precipitated together with aragonite (more soluble than calcite) in the  $\Delta_{\text{an}}$  region. The observation that pLys does not influence the growing space suggests that the increase of supersaturation is a consequence of growth inhibition of calcite crystals and that the nucleation processes are not influenced by the presence of this additive. Indeed, p-Lys is a basic polypeptide ( $pK_a \sim 9$ ) that is positively charged at the pH of the agarose viscous sol. The inhibition process likely takes place after the nucleation event, by electrostatic interaction of the additive with the negatively charged calcite surfaces of crystals formed on the  $\Delta_{\text{an}}$  region (in the presence of an excess of anions), expressing these faces in the growth morphology. Accordingly to this supposed inhibition, a change of the morphology as well as aggregation of calcite crystals was observed with this additive.

The inhibition effect of acidic polypeptides and proteins in the nucleation of calcium carbonate is well-known.<sup>45–48</sup> Here, pAsp, and pGlu to a minor extent, caused an increase of  $t_w$  and  $d_c$  and a strong decrease of  $\Delta$  with respect to the reference. All of these observations are in agreement with the strong inhibition of the nucleation of calcium carbonate. The presence of these two negatively charged additives also caused a strong aggregation of the calcite crystals and a modification of their morphology. These findings indicate that these additives have also an inhibition effect on the growth process.<sup>49</sup>

It is worth noting that, in the presence of pAsp and pGlu, the precipitation of aragonite is not observed, even if conditions of high ionic product activity are present in the viscous sol (see effect of pLys). This observation could be explained considering the strong affinity of pAsp and pGlu for this calcium carbonate polymorph that could provoke the inhibition of its nucleation and further growth.<sup>50,51</sup>

## 6. CONCLUSIONS

We have studied the influence of charged polypeptides, either cationic (pLys) or anionic (pAsp and pGlu), during the precipitation process of calcium carbonate in high viscous agarose sols. It has been found that pLys influences the growth mechanism of calcium carbonate without affecting the nucleation process, whereas pAsp and, to a minor extent, pGlu affect both the nucleation and the growth processes of calcium carbonate. As part of this work, we have defined and measured a number of crystallization parameters ( $x_o$ ,  $t_w$ ,  $\Delta$ ,  $\Delta_{an}$ ,  $\Delta_{an}$ ) that could be used to evaluate the effect of additives on the nucleation and/or growth process of other mineral systems.

## ■ ASSOCIATED CONTENT

### Supporting Information

Graphical representation of the qualitative scale defined to estimate the crystallization density and optical microscope pictures of calcium carbonate precipitates in the agarose viscous sol, in addition to those shown in Figure 5. This material is available free of charge via the Internet at <http://pubs.acs.org>.

## ■ AUTHOR INFORMATION

### Corresponding Author

\*E-mail: giuseppe.falini@unibo.it (G.F.), jaime@lec.csic.es (J.G.-M.).

### Notes

The authors declare no competing financial interest.

## ■ ACKNOWLEDGMENTS

G.F. and S.F. thank the Consorzio Interuniversitario di Ricerca della Chimica dei Metalli nei Sistemi Biologici (CIRC MSB) for the support. M.S.-T., J.G.-M., M.A.D.-O., F.O., and J.M.G.-R. acknowledge the “Factoría de Cristalización” (Consolider Ingenio 2010, Spanish MINECO) and Excellence project RNM5384 of Junta de Andalucía. All authors also thank Dr. García-Caballero for English corrections. M.S.-T. also thanks the CSIC for her JAE-Pre research contract within the “Junta para la Ampliación de Estudios” cofunded by the European Social Fund (ESF).

## ■ ABBREVIATIONS

CDS, counterdiffusion system; pAsp, poly-L-aspartate; pGlu, poly-L-glutamate; pLys, poly-L-lysine;  $\Delta$ , crystal growing space;  $x_{cat}$  and  $x_{an}$ , the boundaries of the crystal growing space close to the cationic and anionic reservoirs, respectively;  $x_o$ , starting point of crystallization;  $\Delta_{cat}$  and  $\Delta_{an}$ , the crystal growing space from the starting point to the cationic and anionic reservoirs, respectively;  $d_o$ , crystallization density;  $t_w$ , waiting time;  $t_n$ , nucleation time;  $t_g$ , growth time

## ■ REFERENCES

- Meldrum, F. C. *Int. Mater. Rev.* **2003**, *48*, 187–224.
- Meldrum, F. C.; Cölfen, H. *Chem. Rev.* **2008**, *108*, 4332–4432.
- Sommerdijk, N. A. J. M.; de With, G. *Chem. Rev.* **2008**, *108*, 4499–4550.
- Peter, K. *The Science and Technology of Industrial Water Treatment*; CRC Press: New York, 2010.
- Lowenstam, H. A.; Weiner, S. *On Biomineralization*; Oxford University Press: New York, 1989.
- Navrotsky, A. *Proc. Natl. Acad. Sci. U.S.A.* **2004**, *101*, 12096–12101.
- Henisch, H. K. *Crystal Growth in Gels*; Pennsylvania State University Press: University Park, PA, 1970.
- Henisch, H. K. *Crystals in Gels and Liesegang Rings*; Cambridge University Press: Cambridge, U.K., 1988.
- Kashchiev, D. *Nucleation: Basic Theory with Applications*; Butterworth-Heinemann: Oxford, U.K., 2000.
- García-Ruiz, J. M.; Míguez, F. *Estud. Geol.* **1982**, *38*, 3–14.
- Henisch, H. K.; García-Ruiz, J. M. *J. Cryst. Growth* **1986**, *75*, 195–202.
- Prieto, M.; Putnis, A.; Fernández-Díaz, L.; López-Andrés, S. *J. Cryst. Growth* **1994**, *142*, 225–235.
- Henisch, H. K.; García-Ruiz, J. M. *J. Cryst. Growth* **1986**, *75*, 203–211.
- Putnis, A.; Prieto, M.; Fernández-Díaz, L. *Geol. Mag.* **1995**, *132*, 1–13.
- Pučar, Z.; Pokrič, B.; Graovac, A. *Anal. Chem.* **1974**, *46*, 403–409.
- García-Ruiz, J. M. *Struct. Biol.* **2003**, *142*, 22–31.
- Iler, R. K. *The Chemistry of Silica*; John Wiley & Sons: New York, 1979.
- Mitchell, J. R.; Blanshard, J. M. V. *J. Texture Stud.* **1976**, *7*, 219–234.
- Rochas, C.; Lahaye, M. *Carbohydr. Polym.* **1989**, *10*, 289–298.
- Otalora, F.; Gavira, J. A.; Ng, J. D.; García-Ruiz, J. M. *Prog. Biophys. Mol. Biol.* **2009**, *101*, 26–37.
- García-Ruiz, J. M. *Key Eng. Mater.* **1991**, *88*, 87–106.
- García-Ruiz, J. M.; Novella, M. L.; Otálora, F. *J. Cryst. Growth* **1999**, *196*, 703–710.
- Fernández-Díaz, L.; Astilleros, J. M.; Pina, C. M. *Chem. Geol.* **2006**, *225*, 314–321.
- Van Driessche, A. E. S.; Otálora, F.; Gavira, J. A.; Sazaki, G. *Cryst. Growth Des.* **2008**, *8*, 3623–3629.
- García-Ruiz, J. M. *Estud. Geol.* **1982**, *38*, 209–225.
- Putnis, A.; Fernández-Díaz, L.; Prieto, M. *Nature* **1992**, *358*, 743–745.
- Li, H.; Xin, H. L.; Muller, D. A.; Estroff, L. A. *Science* **2009**, *326*, 1244–1247.
- Kellermeier, M.; Cölfen, H.; García-Ruiz, J. M. *Eur. J. Inorg. Chem.* **2012**, *5123–5144*.
- Grassmann, O.; Neder, R. B.; Putnis, A.; Löbmann, P. *Am. Mineral.* **2003**, *88*, 647–652.
- Kosanović, C.; Falini, G.; Kralj, D. *Cryst. Growth Des.* **2011**, *11*, 269–277.
- Asenath-Smith, E.; Li, H.; Keene, E. C.; Seh, Z. W.; Estroff, L. A. *Adv. Funct. Mater.* **2012**, *22*, 2891–2914.
- Dorvee, J. R.; Boskey, A. L.; Estroff, L. A. *CrystEngComm* **2012**, *14*, 5681–5700.
- Geckil, H.; Xu, F.; Zhang, X.; Moon, S.; Demirci, U. *Nanomedicine* **2010**, *5*, 469–484.
- Silverman, L.; Boskey, A. L. *Calcif. Tissue Int.* **2004**, *75*, 494–501.
- Iafisco, M.; Marchetti, M.; Gómez-Morales, J.; Hernández-Hernández, A.; García-Ruiz, J. M.; Roveri, N. *Cryst. Growth Des.* **2009**, *9*, 4912–4921.
- Sánchez-Pastor, N.; Gigler, A. M.; Cruz, J. A.; Park, S.-H.; Jordan, G.; Fernández-Díaz, L. *Cryst. Growth Des.* **2011**, *11*, 3081–3089.
- Fernández-Díaz, L.; Putnis, A.; Prieto, M.; Putnis, C. V. *J. Sediment. Res.* **1996**, *66*, 482–491.
- García-Ruiz, J. M.; Novella, M. L.; Moreno, R.; Gavira, J. A. *J. Cryst. Growth* **2001**, *232*, 165–172.

- (39) Vinograd, J. R.; McBain, J. W. *J. Am. Chem. Soc.* **1941**, *63*, 2008–2015.
- (40) Appelo, C. A. J.; Wersin, P. *Environ. Sci. Technol.* **2007**, *41*, 5002–5007.
- (41) Parkhurst, D. L.; Appelo, C. A. J. *User's Guide to PHREEQC (Version 2): A Computer Program for Speciation, Batch-Reaction, One-Dimensional Transport and Inverse Geochemical Calculations*; U.S. Geological Survey Water-Resources Investigations Report 99-4259; U.S. Geological Survey: Reston, VA, 1999.
- (42) Jones, G. C.; Jackson, B. *Infrared Transmission Spectra of Carbonate Minerals*; Chapman & Hall: London, 1993.
- (43) Falini, G.; Fermani, S.; Tosi, G.; Dinelli, E. *Cryst. Growth Des.* **2009**, *9*, 2065–2072.
- (44) Gómez-Morales, J.; Torrent-Burgués, J.; López-Macipe, A.; Rodríguez-Clemente, R. *J. Cryst. Growth* **1996**, *166*, 1020–1026.
- (45) Njegić-Džakula, B.; Brečević, L.; Falini, G.; Kralj, D. *Cryst. Growth Des.* **2009**, *9*, 2425–2434.
- (46) Hernández-Hernández, A.; Gómez-Morales, J.; Rodríguez-Navarro, A. B.; Gautron, J.; Nys, Y.; García-Ruiz, J. M. *Cryst. Growth Des.* **2008**, *8*, 4330–4339.
- (47) Hernández-Hernández, A.; Rodríguez-Navarro, A. B.; Gómez-Morales, J.; Jiménez-López, C.; Nys, Y.; García-Ruiz, J. M. *Cryst. Growth Des.* **2008**, *8*, 1495–1502.
- (48) Goffredo, S.; Vergni, P.; Reggi, M.; Caroselli, E.; Sparla, F.; Levy, O.; Dubinsky, Z.; Falini, G. *PLoS One* **2011**, *6*, e22338.
- (49) Addadi, L.; Weiner, S. *Proc. Natl. Acad. Sci. U.S.A.* **1985**, *82*, 4110–4114.
- (50) Stephenson, E.; De Yoreo, J. J.; Wu, L.; Wu, K. J.; Hoyer, J.; Dove, P. M. *Science* **2008**, *322*, 724–727.
- (51) Weiner, S.; Addadi, L. *Annu. Rev. Mater. Res.* **2011**, *41*, 21–40.